High Yield Silicon Photonic Crystal Microcavity Biosensors with 100fM Detection Limit

Yi Zou*[, a], Swapnajit Chakravarty*[, b], Wei-Cheng Lai[a], Cheng-Chih Hsieh[a], Ray T. Chen*[, a]
[a]Dept. of Electrical and Computer Engineering, University of Texas, 10100 Burnet Road Bldg. 160, Austin, TX, USA 78758; [b]Omega Optics Inc., 10306 Sausalito Drive, Austin, TX, USA 78759

ABSTRACT

We experimentally demonstrated a silicon photonic crystal (PC) microcavity biosensor with 50 femto-molar detection limit. Our devices have demonstrated sensitivities higher than than competing optical platforms at concentration of 0.1μg/ml across a range of dissociation constants KD 1 micro-molar to 1 femto-molar. High sensitivities were achieved by slow light engineering which reduced the radiation loss and increased the stored energy in the PC microcavity resonance mode which contributed to high Q as well as enhanced optical mode overlap with the analyte. By integrating subwavelength grating coupler, we showed that not only coupling efficiency increased but also the working device yield significantly improved

Keywords: photonic crystal waveguide, photonic crystal microcavity, biosensor, sub-wavelength grating coupler.

*yzou@utexas.edu, swapnajit.chakravarty@omegaoptics.com, raychen@uts.cc.utexas.edu; phone 1 512 471-4349; fax 1 512-471-8575;

1. INTRODUCTION

Silicon photonics is a promising platform for high density integration of photonic devices. It is compatible with CMOS fabrication and therefore high volume manufacturing is feasible. In spite of several performance advantages, coupling of light into and out of silicon devices reliably has been a primary impediment towards large scale adoption of silicon photonics to real applications. Optical fibers have been the primary guiding medium for light into and out of the photonic chips. However, due to large mode and effective index mismatches between fiber and silicon waveguide, dimensions of which are of the order of several hundred nanometers, silicon based optical devices suffer very high loss when coupling light into/out from chips. In order to solve this problem, several coupling approaches have been proposed. Two methods typically adopted are inverse tapers [1, 2, 3, 4] and grating couplers which include traditional air trench grating design [5, 6, 7, 8, 9, 10] and sub-wavelength nanostructures [11, 12, 13, 14, 15, 16]. The results demonstrated that among the competing methods, coupling efficiency can be significantly improved in sub-wavelength grating couplers which provide a lot of design freedom to meet the requirement of different applications. Recent work has also shown that the special designed sub-wavelength grating coupler for TE polarization can be fabricated simultaneously with the other photonic devices thus adding no additional step for fabrication, and achieve very high coupling efficiency [15]. Since transverse-electric (TE) polarization is the polarization state we need to guide inside 2-D silicon photonic crystal waveguides, by adding a TE selected sub-wavelength grating coupler we actually have an additional polarization filter that can further increase the extinction ratio between TE and TM polarizations inside our waveguide. In recent years, photonic crystal (PC) microcavities, because of its compact size (of the order of a few square microns in surface area) and high sensitivity, have attracted significant interest in bio-sensing. The working mechanism is based on transducing the specific binding of the biomolecule of interest to its conjugate biomolecule receptor bound to the photonic crystal microcavity into an optical signal. Compared to other competitors such as ring-resonators [17, 18], wire waveguides [19] and surface plasmon resonance (SPR) [20], PC microcavities have higher sensitivity due to its slow light effect, high quality factor resonances and a larger optical mode overlap with the analyte within compact optical mode volume [21]. However, in spite of significant success in demonstrating highest sensitivity biosensors [22], working device yield using end-fire coupling, after successful fabrication was dismal, of the order of 10% in some instances [23].

In this letter, we integrated sub-wavelength grating couplers and PC microcavity coupled waveguides for bio-sensing. Not only is coupling efficiency increased compared to previous end-fire coupling methods, but also the working device yield is significantly improved to 70% with significantly improved spectral purity of observed resonances. We

Frontiers in Biological Detection: From Nanosensors to Systems V, edited by Benjamin L. Miller, Philippe M. Fauchet, Proc. of SPIE Vol. 8570, 857008
 · doi: 10.1117/12.2005149

experimentally detected sensitivity more than one order of magnitude better than our previous results [22]. Our preliminary yield results combining sub-wavelength grating couplers with PC microcavity coupled waveguides are extremely significant for bio-sensing microarray applications that will consider dense integration of multiple simultaneously interrogated sensors on chip [24].

2. DEVICE DESIGN

A. Device Principles of Sub-wavelength Grating Coupler

The sub-wavelength grating coupler works on the same principle as the traditional grating coupler except it replaces the air trenches with a sub-wavelength nanostructure, as shown in Fig.1(a). According to effective medium theory (EMT) [25], if a composite medium comprises two different materials interleaved at the sub-wavelength scale, it can be treated approximately as a homogenous medium with an effective refractive index between these two materials. Based on these two working principles, the sub-wavelength grating coupler covered by SU8 protection layer was simulated by two-dimensional simulation package CAMFR using the design rules laid down previously [15]. The combination of grating period and effective refractive index were scanned to get the maximum upward coupling efficiency through sub-wavelength grating. The simulation result is shown in Fig.1(b).
As we can see, when the grating period Λ_G is fixed at 735nm and the effective refractive index of sub-wavelength region is set as 2.15 which are indicated in Fig. 1(b), the upward coupling efficiency to air reaches its maximum which is around 26% with an emitting angle of 14 o. The duty cycle is 50% while 22 periods are chosen to make the grating region 14 μm wide and 16 μm long that can match well with the mode size of a single mode fiber and also provide some tolerances to make the alignment easily [11]. The values for parameters Λ_{sub} and W_{sub} are calculated according to 1D stratified structure [26]. And considering fabrication yield and repeatability limitations, we set the trench width W_{sub}=100nm and thus we can fix the parameter Λ_{sub}=294nm which corresponds to a filling factor around 34%.

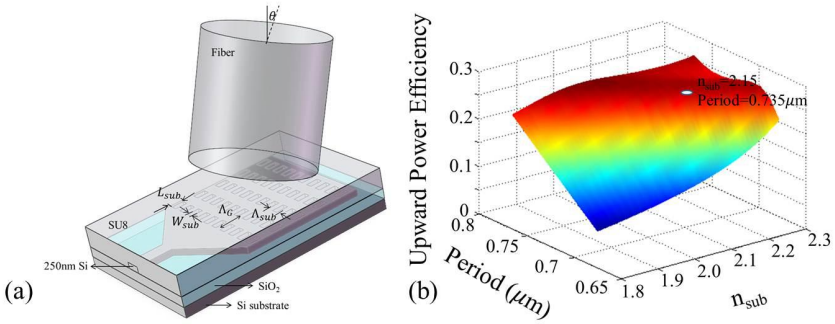

Fig. 1. (a) A schematic of sub-wavelength grating coupler. (b) Upward power efficiency as a function of grating period Λ_G and the effective refractive index n_{sub} of the sub-wavelength structure.

B. Principles of Group Index Based Photonic Crystal Microcavities

The device investigated is a L_n type PC microcavity side coupled to a W1 Photonic Crystal waveguide (PCW), where n denotes the number of missing air holes along the Γ–K lattice direction in a triangular lattice Photonic Crystal and W1 demotes that the width of the PCW is √3a. The schematic of PC device is shown in Fig. 2(a).

The total quality factor Q_T of the resonance mode of a PC microcavity side coupled to a PCW, which is related to the photon lifetime τ_p, at frequency ω by $Q_T=\omega\tau_p$ is given by

$$\frac{1}{Q_T}=\frac{1}{Q_i}+\frac{1}{Q_R}+\frac{1}{Q_{WG}} \quad \ldots\ldots\ldots\ldots (1)$$

where $Q_R=\omega\tau_R$, $Q_i=\omega\tau_i$, and $Q_{WG}=\omega\tau_{WG}$, τ_R, τ_i and τ_{WG} represent time constants for the radiation loss, intrinsic cavity loss and waveguide loss respectively. τ_R is given by:

$$\frac{1}{\tau_R} = \frac{P_R}{W_E} \quad \text{..... (2)}$$

where P_R denotes the total power radiated by the cavity and W_E denotes the stored energy in the cavity which is proportional to the cavity mode volume. Hence a method that reduces P_R and increases W_E will decrease the radiation loss from the cavity and hence increase the effective Q. A higher Q implies that the light is trapped for a longer period of time in the cavity and hence interacts longer with any analyte in the vicinity of the PC microcavity. In addition, since WE is proportional to the optical mode volume, a higher WE leads to potential for larger optical mode overlap with the analyte which also contributes to higher sensitivity. Since the sensitivity of the device is determined by the resonance wavelength shift needed to observe the smallest change in concentration, a large resonance wavelength shift is desired for a given concentration of chemicals or biomolecules. We have shown previously [23] that the resonance wavelength shift can be enhanced by increasing both the Q and the analyte overlap with the resonance mode of the microcavity.

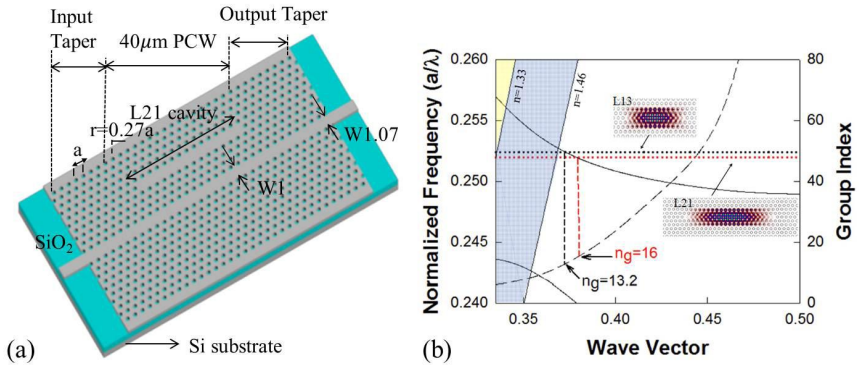

Fig. 2. (a) A schematic of photonic crystal microcavity device, (b) dispersion diagram of W1 PCW in water. The W1 guided mode is shown together with frequencies of resonant modes for L13 and L21 PC microcavities by black and red dashed lines respectively. The mode profiles are shown in insets.

3. EXPERIMENTAL RESULTS

To characterize the performance, devices were tested on a measurement setup described in a previous paper [15]. Input light from a broadband amplified spontaneous emission (ASE) source (Thorlabs ASE-FL7002) covering the 1520–1610 nm wavelength range was TE-polarized and coupled to and from the sub-wavelength grating with a polarization maintaining single mode fiber. Light is guided in and out of the PCW by ridge waveguide with PC group index taper to enable high coupling efficiency into the slow light guided mode. The bottom cladding of silicon dioxide (n=1.46) is kept intact to enable robust devices with high yield. The sub-wavelength grating coupler is firstly characterized by measuring the insertion loss of fiber-to-device-to-fiber and the coupling efficiencies of two couplers are assumed as equal. Therefore we can get the efficiency of one grating as shown in Fig. 3. The curve indicates that the peak efficiency for one sub-wavelength grating coupler is around -7dB which corresponding to 20% efficiency at 1550nm and the 3dB bandwidth is around 53nm. The efficiency drop compared to previous reported data [15] is due to the SU8 top cladding of grating region which serves as the protection layer to eliminate any interference to the grating signal due to analyte spreading during bio-sensing. The output spectrum of the grating was used as reference for the whole device characterization.

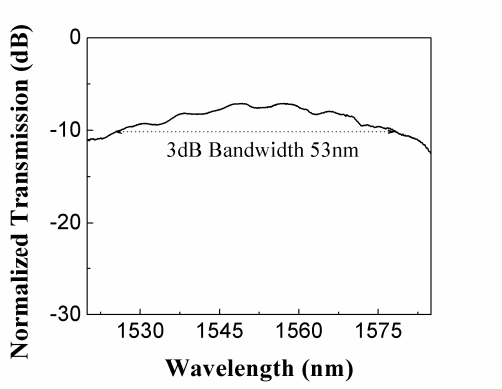

Fig. 3. Normalized transmission of one sub-wavelength grating.

In order to test the repeatability, we made 10 L21 devices on a chip and measured all the spectra under water and glycerol. Nine out of ten devices give similar output power as well as good spectra, all spectra show clear and sharp transmission band edges, of which the power drop almost 30dB within 5nm range during the transition from transmission band to band gap. The spectra from each of the nine devices in glycerol are shown in Fig. 4(a). The output power from each of the devices is shown in Fig. 4(b). Inside the transmission bands, the spectra are very smooth with less than 2dB of Fabry-Perot effect, so the resonant modes are easy to distinguish. The absolute wavelength positions of all the resonant modes and band edges are very close to each other, the slight difference may be due to fabrication errors or the different thicknesses of the SOI wafer at the specific location of the photonic crystal pattern on the SOI wafer. The bulk sensitivity of a resonance mode is calculated for the resonant mode closest to the band edges in all nine devices in spectrum of Fig. 5(a), by comparing the resonance wavelength position in water and glycerol. The bulk sensitivities also show good consistency across devices being roughly around 72nm/RIU as can be seen from Fig. 5(c). We also provide the output power and spectrum of Device 5 in Fig. 4(b) and Fig. 4(d) respectively. The transmission of this device is much lower than others, and its spectrum has Fabry-Perot resonances separated roughly 6nm away from each other overlapped with the PC microcavity resonance modes. We believe that the transmission power drop is contributed by a defect on the stripe waveguide section to Device 5, as shown in the SEM image in Fig. 4(f).

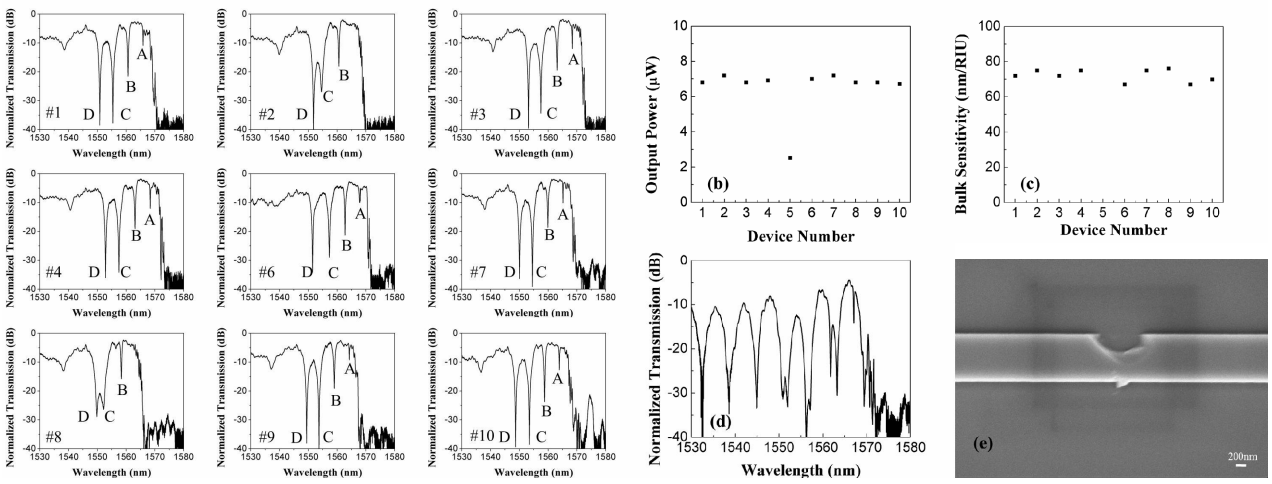

Fig. 4. (a) Experimental transmission spectra in glycerol of 9 out of 10 devices comprising W1 PCW coupled to L21 PC microcavities. (b) Output power of all ten L21 devices, (c) bulk sensitivity of 9 devices, (d) transmission spectrum of L21 device #5 (d) SEM image of defect on ridge waveguide section at the input of PCW in Device 5.

4. BIOSENSING RESULTS

The biomolecule functionalization process has been described in detail in ref. [22]. 60μl target protein Avidin (67kDa) solution was directly dispensed from a micro-pipette. The diameter of the dispensed spot on silicon is around 8mm. During biosensing measurements, after each new addition of a new concentration of target protein, the device is washed

three times in PBS and the effective resonance wavelength shift is measured. Experimental resonance transmission spectra observed when avidin binds to the probe biotin is shown in Fig. 5(a). The lowest concentrations are shown separately in Fig. 5(b) for clarity. At the lowest concentration of 1pM which corresponds to 67pg/ml avidin, a resonance wavelength shift of 0.04nm was observed as shown in Fig. 5(b). In the L21 PC microcavity, (integrating over an area where the E-field intensity is more than 50% of the maximum value and including the entire internal surface area of the holes along the periphery of the photonic crystal microcavity in the Γ−K orientation where the E-field intensity is more than 50% over a fraction of the periphery of the hole) [27], from Fig. 2(b), the optical mode overlaps a surface area on the chip of 13.62μm^2. The actual real estate coverage of the optical mode on the chip is approximately 5.7μm^2 similar to the L13 PC microcavity [22]. By assuming uniform surface coverage, the detection limit for surface density is 80fg/mm^2. Fig. 5(c) plots the resonant wavelength shift Δλ as a function of concentration. To verify sensing repeatability, two identical L21 PC microcavity coupled PCW devices were fabricated and tested. Both show similar wavelength shift when different concentrations were added. These results further prove the measurement repeatability of L21 PC microcavity devices. A control experiment is done to verify that no resonance wavelength shift occurs in a control PC microcavity coated with BSA when different concentrations of avidin are introduced. The wavelength shifts observed in the control experiments are within 0.02nm, which is within the wavelength accuracy limit of our optical spectrum analyzer. Consequently, in all sensing experiments, resonance wavelength shifts greater than 0.02nm were considered as the signature of a binding event between the receptor capture biomolecule and its specific conjugate.

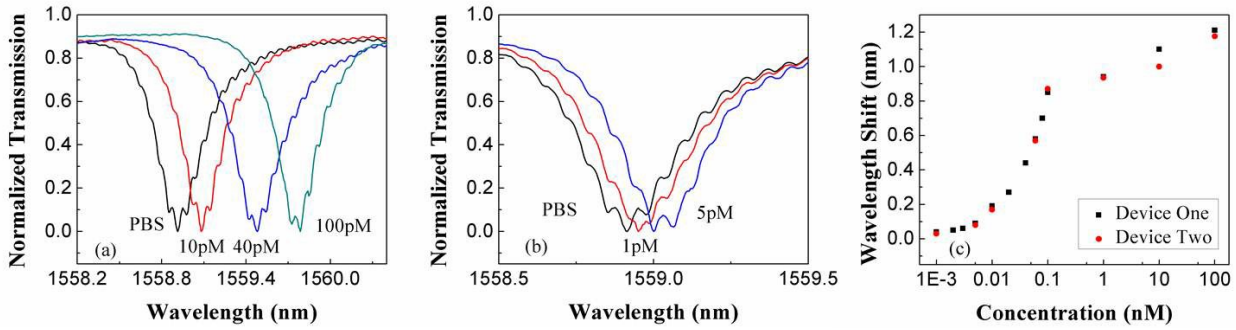

Fig. 5. Experimental drop resonance spectra for the binding between Avidin to Biotin (Kd~10^{-15}M) (a) between 0pM to 100pM and (b) at the lower concentration range between 0pM and 5pM. (c) Experimental spectral shift for various concentrations of avidin binding to biotin in two L21 (filled circles and filled squares) PC microcavities.

We also made a L55 PC microcavity device. In this case the cavity size was increased to around 20μm, but it is still less than 35μm which is the drop size of our inkjet-printed probe protein. We did biosensing on this device following the same procedure as for L21 devices, and we successfully detected Avidin-Biotin binding at the concentration of 50 femto-Molar that further extends the detection limitation more than one order than our previous results.

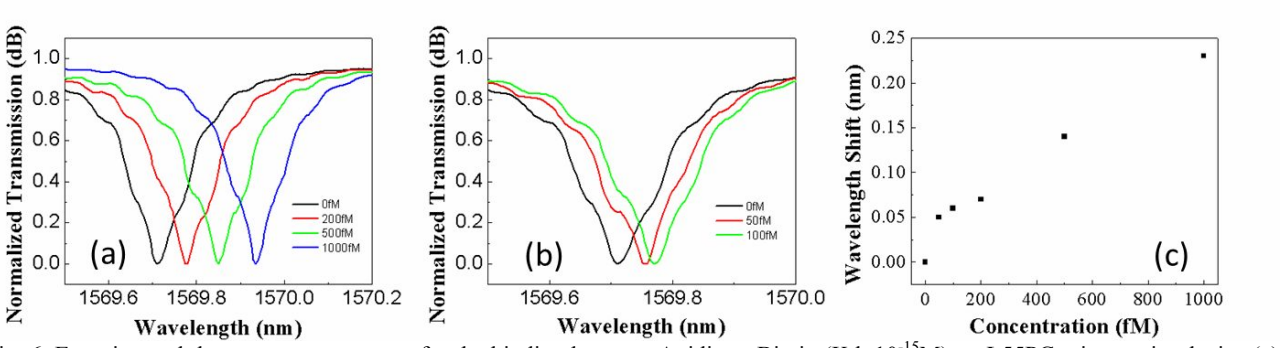

Fig. 6. Experimental drop resonance spectra for the binding between Avidin to Biotin (Kd~10^{-15}M) on L55PC microcavity device (a) between 0fM to 1000fM and (b) at the lower concentration range between 0fM and 100fM. (c) Experimental spectral shift for various concentrations of avidin binding to biotin in L55 PC microcavities.

5. SUMMARY

In summary, we demonstrated an on-chip sensing system for high yield and high sensitivity bio-sensing combining sub-wavelength grating couplers and L21 and L55 PC microcavity side-coupled to PCW. In addition to high device yields, of 70% successful rate for L21 devices, sub-wavelength grating couplers also significantly improve the quality of the resonance spectrum. Future devices will further investigate lower yield issues observed in L21 PC microcavities. The experimentally detected the binding of 1pM and 50femto-molar concentration of avidin to its specific conjugate biotin in PBS for L21 and L55 devices respectively, at least one order of magnitude higher than our previous demonstration [22] and with higher sensitivity than other competing technologies. Device miniaturization is still retained from the context of practical engineering limitations of biomolecule patterning in a biosensing microarray. The sensing area of our device is smaller than other techniques such as nano-hole plasmonic arrays [28], or surface enhanced Raman scattering sensors [29] at equivalent detected concentrations, which essentially interrogate the signal over a large number of hot spots to achieve published sensitivities.

ACKNOWLEDGEMENTS

This work was supported by the National Cancer Institute SBIR Contract #HHSN261201000085C. We further acknowledge AFOSR MURI for the silicon nanomembrane research works (Contract # FA9550-08-1-0394).

REFERENCES

[1] T. Shoji, T. Tsuchizawa, T. Watanabe, K. Yamada, and H. Morita, "Low loss mode size converter from 0.3 μm square Si wire waveguides to single mode fibers," Electron. Lett. 38, 1669-1670 (2002).
[2] V. R. Almeida, R. R. Panepucci, and M. Lipson, "Nanotaper for compact mode conversion," Opt. Lett. 28, 1302-1304 (2003).
[3] K. K. Lee, D. R. Lim, D. Pang, C. Hoepfner, W-Y. Oh, K. Wada, L. C. Kimerling, K. P. Yap, and M. T. Doan, "Mode transformer for miniaturized optical circuits," Opt. Lett. 30, 498-500 (2005).
[4] S. J. McNab, N. Moll, and Y. A. Vlasov, "Ultra-low loss photonic integrated circuit with membrane-type photonic crystal waveguides," Opt Express **11** (22), 2927 (2003).
[5] D. Taillaert, F. Van Laere, M. Ayre, W. Bogaerts, D. Van Thourhout, P. Bienstman, and R. Baets, "Grating Couplers for Coupling between Optical Fibers and Nanophotonic Waveguides," Jpn. J. Appl. Phys. 45, 6071–6077 (2006).
[6] Y. Tang, Z. Wang, L. Wosinski, U. Westergren, and S. He, "Highly efficient nonuniform grating coupler for silicon-on-insulator nanophotonic circuits," Opt. Lett. 35, 1290–1292 (2010).
[7] G. Roelkens, D. Vermeulen, D. Van Thourhout, R. Baets, S. Brision, P. Lyan, P. Gautier, and J. M. F´ed´eli, "High efficiency diffractive grating couplers for interfacing a single mode optical fiber with a nanophotonic silicon-on-insulator waveguide circuit," Appl. Phys. Lett. 92, 131101 (2008).
[8] F. Van Laere, G. Roelkens, M. Ayre, J. Schrauwen, D. Taillaert, D. Van Thourhout, T. F. Krauss, and R. Baets, "Compact and Highly Efficient Grating Couplers Between Optical Fiber and Nanophotonic Waveguides," Lightwave Technology, Journal of 25 (1), 151 (2007).
[9] M. Antelius, K. B. Gylfason, and H. Sohlström, "An apodized SOI waveguide-to-fiber surface grating coupler for single lithography silicon photonics," Opt. Express 19 (4), 3592 (2011).
[10] F. Li, L. Wu, T. Li, M. Dubinovsky, S. Tang, Ray T. Chen, "Unidirectional surface-normal waveguide grating coupler for wafer-scale MCM interconnect," SPIE Proc. Vol. 3005, Optoelectronics 1997, San Jose, CA, Feb. 10-14, 1997.
[11] L. Liu, M. Pu, K. Yvind, and J. M. Hvam, "High-efficiency, large-bandwidth silicon-on-insulator grating coupler based on a fully-etched photonic crystal structure," Applied Physics Letters 96 (5), 051126 (2010).
[12] R. Halir, P. Cheben, S. Janz, D.-X. Xu, Í. Molina-Fernández, and J. G. Wangüemert-Pérez, "Waveguide grating coupler with subwavelength microstructures," Opt. Lett. 34 (9), 1408 (2009).
[13] R. Halir, P. Cheben, J. H. Schmid, R. Ma, D. Bedard, S. Janz, D. X. Xu, A. Densmore, J. Lapointe, and ´I. Molina-Fern´andez, "Continuously apodized fiber-to-chip surface grating coupler with refractive index engineered subwavelength structure," Opt. Lett. 35, 3243–3245 (2010).

[14] C. Xia and H. K. Tsang, “Nanoholes grating couplers for coupling between silicon-on-insulator waveguides and optical fibers,” Photonics Journal, IEEE 1 (3), 184 (2009).
[15] X. Xu, H. Subbaraman, J. Covey, D. Kwong, A. Hosseini, and Ray T. Chen, “Complementary metal–oxide–semiconductor compatible high efficiency subwavelength grating couplers for silicon integrated photonics,” Applied Physics Letters **101**, 031109 (2012).
[16] H. Subbaraman, X. Xu, J. Covey, and Ray T. Chen, "Efficient light coupling into in-plane semiconductor nanomembrane photonic devices utilizing a sub-wavelength grating coupler," Optics Express, 20(18), 20659-20665 (2012)
[17] M. Iqbal, M. A. Gleeson, B. Spaugh, F. Tybor, W. G. Gunn, M. Hochberg, T. Baehr-Jones, R. C. Bailey, and L. C. Gunn, “Label-free biosensor arrays based on silicon ring resonators and high-speed optical scanning instrumentation,” IEEE J. Sel. Top. Quant. Electron. 16, 654 (2010).
[18] C. F. Carlborg, K. B. Gylfason, A. Kazmierczak, F. Dortu, M. J. Banuls Polo, A. Maquieira Catala, G. M. Kresbach, H. Sohlstrom, T. Moh, L. Vivien, J. Popplewell, G. Ronan, C. A. Barrios, G. Stemme, and W. van der Winjgaart, “A packaged optical slot-waveguide ring resonator sensor array for multiplex label-free assays in labs-on-chips,” Lab Chip 10, 281 (2010).
[19] A. Densmore, M. Vachon, D. X. Xu, S. Janz, R. Ma, Y. H. Li, G. Lopinski, A. Delage, J. Lapointe, C. C. Luebbert, Q.Y. Liu, P. Cheben, and J.H. Schmid, “Silicon photonic wire biosensor array for multiplexed real-time and label-free molecular detection,” Opt. Lett. 34, 3598 (2009).
[20] H. Sipova, S. Zhang, A. M. Dudley, D. Galas, K. Wang, and J. Homola, “Surface plasmon resonance biosensor for rapid label-free detection of microribonucleic acid at subfemtomole level,” Anal. Chem. 82, 10110 (2010).
[21] B. S. Song, S. Noda, T. Asano and Y. Akahane, “Ultra-high-Q photonic double heterostructure nanocavity”, Nat. Mater. 4, 3, 207 (2005).
[22] S. Chakravarty, Y. Zou, W. Lai, and Ray T. Chen, “Slow light engineering for high Q high sensitivity photonic crystal microcavity biosensors in silicon,” Biosensors and Bioelectronics 38(1), 170-176 (2012).
[23] W. C. Lai, S. Chakravarty, Y. Zou and R. T. Chen, “Silicon nano-membrane based photonic crystal microcavities for high sensitivity bio-sensing,” Optics Lett. 37, 1208-1210 (2012).
[24] Y. Zou, S. Chakravarty, W. Lai, C. Lin and Ray T. Chen, “Methods to array photonic crystal microcavities for high throughput high sensitivity biosensing on a silicon-chip based platform,” Lab on a Chip, 12(13), 2309-2312 (2012).
[25] P. Yeh, A. Yariv, and C.-S. Hong, “Electromagnetic propagation in periodic stratified media. I. General theory,” J. Opt. Soc. Am. 67 (4), 423 (1977).
[26] S. M. Rytov, “Electromagnetic properties of a finely stratified medium,” Sov. Phys. JETP 2 (3), 10 (1956).
[27] D. Dorfner, T. Zabel, T. Hürlimann, N. Hauke, L. Frandsen, U. Rant, G. Abstreiter, J. Finley, “Photonic crystal nanostructures for optical biosensing applications,” Biosensors and Bioelectronics, 24(12),3688–3692, (2009).
[28] T-Y Chang, M. Huang, A. A. Yanik, H-Y Tsai, P. Shi, S. Aksu, M. F. Yanik and H. Altug, “Large-Scale Plasmonic Microarrays for Label-Free High-Throughput Screening,” Lab on a Chip, 11, 3596-3602 (2011).
[29] Z. Chen, S. M. Tabakman, A. P. Goodwin, M. G. Kattah, D. Daranciang, X. R. Wang, G. Y. Zhang, X. L. Li, Z. Liu, P. J. Utz, K. L. Jiang, S. S. Fan and H. J. Dai, “Protein microarrays with carbon nanotubes as multicolor Raman labels,” Nat. Biotechnol., 26, 1285–1292 (2008).